

Sunyaev-Zeldovich effect from hydrodynamical simulations: maps and low order statistics

Uroš Seljak, Juan Burwell

Department of Physics, Jadwin Hall, Princeton University, Princeton, NJ 08544

Ue-Li Pen

Canadian Institute of Theoretical Astrophysics, University of Toronto, 60 St. George St., Toronto, Canada;

pen@cita.utoronto.ca

(Submitted to PRD - January 2000)

We use moving mesh hydrodynamical simulations to make maps of Sunyaev-Zeldovich effect. We present these maps for several cosmological models and explore their lowest moments. We find that the first moment, the mean Compton y parameter, is typically between $1 - 2 \times 10^{-6}$ for cluster abundance normalized models, the lower value corresponding to the high density models, and scales as σ_8^{3-4} . Rms fluctuations at $10'$ scale have an amplitude $\Delta T/T \sim 1 - 3 \times 10^{-6}$ in the Rayleigh-Jeans regime. The amplitude of the power spectrum strongly depends on the power spectrum normalization and scales as σ_8^{6-9} . On smaller scales ($l > 1000$) the spectrum is dominated by halos below $10^{13} M_\odot$ and so is sensitive to the thermal history of galactic halo gas. On larger scales ($l < 1000$) the power spectrum is less sensitive to nongravitational energy injection, but becomes very noisy, with large field to field variations in the power spectrum caused by rare bright sources in the maps, which dominate in the spectrum over the large scale structure correlations. Cross-correlation power spectrum with weak lensing or projected galaxy distribution is significant and the cross-correlation coefficient is around 0.5 over a wide range of scales. Comparison with Press-Schechter predictions gives very good agreement for all the statistics, indicating that there is no significant contribution to SZ from non-virialized structures. The one point distribution function shows clear deviations from gaussianity and can be well-approximated as log-normal on small scales.

I. INTRODUCTION

Cosmic microwave background (CMB) photons propagating through the universe are scattered by hot electrons along their path. The effect of this scattering on the photon distribution was first described by Sunyaev and Zeldovich [1] and is called the Sunyaev-Zeldovich (SZ) effect. The effect conserves the number of photons, but changes their energy distribution. Low frequency photons in the Rayleigh-Jeans regime gain energy on average and are moved into the high frequency part of the Planck distribution, with a zero crossing at 217GHz in the nonrelativistic case. The amplitude of the effect is proportional to the product of electron temperature and density, or pressure, and is thus dominated by hot dense structures such as clusters.

The SZ effect is nowadays routinely detected by a number of instruments such as BIMA, Diabolo, OVRO, PRONAOS, Ryle, SEST, SuZie and Viper (see refs. [2,3] for review). All of these have so far concentrated their efforts on known clusters, but future experiments will also observe blank fields of the sky with an effort to isolate this effect. Among these are the proposed one square degree survey [4] and a number of CMB experiments, for which SZ may be a significant source of fluctuations that needs to be separated from the primary signal. The Planck satellite for example, with its combination of frequency coverage, all-sky map and angular resolution, should be able to identify several thousand SZ sources [5].

The SZ effect has a number of potentially observable consequences in addition to the one described above on the known clusters. First, the mean SZ distortion can be observed through the deviation of the photon spectrum from the Planck distribution. No such distortion has been detected by the COBE/FIRAS data yielding the upper limit on Comptonization parameter y (defined below) of $y < 1.5 \times 10^{-5}$ [6]. This is a constraint that has to be satisfied by any viable cosmological model. As we will show below cluster abundance normalized models explored here typically satisfy this constraint.

Second, most of the CMB experiments measure fluctuations, for which the most relevant quantity is their power spectrum. Again no clear detection of SZ has been reported so far, although this is not unexpected given that the main source of fluctuations on degree scales probed so far are primary CMB fluctuations generated at the time of recombination. The next generation of CMB experiments is beginning to detect fluctuations at smaller angular scales. With higher sensitivities and broader frequency coverage SZ may become detectable even in random patches of the sky surveyed by these experiments. There are two related questions that one would like to address. First is the overall level of SZ fluctuations and whether SZ may be a significant source of CMB foreground contamination. Second is

the power of SZ to distinguish between cosmological models using power spectrum or any other statistics, such as counting of sources or nongaussian signatures.

There are two main theoretical approaches that can be used when calculating the SZ effect. One is analytical and is based on the Press-Schechter approximation. In this approach all the mass in the universe is distributed into virialized halos. Gas in these halos is assumed to follow a prescribed distribution in density and temperature (usually isothermal with a β density profile). One then integrates over the mass function and over the redshifts to calculate the first moment of the distribution (the y parameter). A similar calculation also yields the uncorrelated contribution to the second moment [7] to which one must also add the correlations between the halos [8,9]. This approach involves a number of approximations that must be verified with numerical simulations. For example, some fraction of the gas may not be in virialized halos, but may be residing in more diffuse filaments or at the outskirts of the halos. There may be significant temperature and density fluctuations of the gas inside the halos. Furthermore, N-body simulations that have examined the accuracy of the Press-Schechter mass function have shown it to be a reasonable approximation for massive halos, but to overpredict the number of halos at lower masses. The resulting spectrum may be very sensitive to the details of the mass function distribution.

The alternative approach adopted in this paper is to use numerical simulations to calculate the SZ effect. Our approach is based on moving mesh hydrodynamical simulation code [10] and we use ray tracing through the simulation box to generate maps of SZ. This is the approach that was adopted previously by [11,12]. Most of these early studies were of low resolution, but nevertheless showed that SZ could be an important effect on the CMB. Recently [13] generated SZ maps using SPH simulations of higher resolution, although they did not calculate the CMB power spectra. An alternative method based on $3-d$ power spectra was developed in [14] and was recently adopted to the MMH code as used in this paper by [15]. We compare our results to the previous work where possible.

II. METHOD

We use moving mesh hydro (MMH) code developed by one of us [10]. The code is a hybrid between Eulerian and Lagrangian grid based hydrodynamic methods. By deforming the grid in the dense regions along potential flow lines it provides a ten fold increase in resolution compared to fixed grid Eulerian codes, while maintaining regular grid conditions everywhere [10]. The code has been successfully parallelized on shared memory systems and has a low computational cost per grid cell. A 256^3 run takes around 2-4 days of wall clock time on 32 processors.

We ran about a dozen simulations varying cosmological parameters, box sizes and particle/mesh dimensions to check for various numerical effects. Our main models are τ CDM, Λ CDM and OC DM. Their parameters are

- τ CDM: flat model with $\Omega_m = 1$, $\Omega_\Lambda = 0$, $\sigma_8 = 0.56$, $\Omega_b h = 0.034$ and $\Omega_m h = 0.25$.
- Λ CDM: flat model with $\Omega_m = 0.37$, $\Omega_\Lambda = 0.63$, $\sigma_8 = 0.8$, $\Omega_b h = 0.034$ and $\Omega_m h = 0.25$.
- OC DM: open model with $\Omega_m = 0.37$, $\Omega_\Lambda = 0.0$, $\sigma_8 = 0.8$, $\Omega_b h = 0.034$ and $\Omega_m h = 0.25$.

We ran several simulations varying box sizes from $50h^{-1}$ Mpc to $200h^{-1}$ Mpc to verify the effects of mass and force resolution on small scales and lack of power on large scales. We also varied mass and scale resolution, using mesh sizes between 128^3 and 256^3 and typically placing 1-8 dark matter particles per mesh cell. Our largest simulations are Λ CDM and OC DM models with $100h^{-1}$ Mpc box, 256^3 mesh and 256^3 dark matter particles.

During the simulation we store 2-d projections through the 3-d box at every conformal time step that corresponds to a light crossing time through the box. The projections are made alternatively in x , y and z direction to minimize the repetition of the same structures in projection. We store projections of SZ, kinetic SZ, gas and dark matter density. For SZ we store the projection

$$\Delta y = \frac{k_B \sigma_T}{m_e c^2} n_e T_e a \Delta \chi \quad (1)$$

where σ_T is the Thomson cross-section, c the speed of light, m_e the electron mass, $\Delta \chi$ the comoving width of the box, a the expansion factor, n_e electron number density and T_e electron temperature, both of which are obtained from the output of the MMH hydro code (note that we ignore relativistic corrections, which are only relevant for rare hot clusters). Our 2-d maps are 1024^2 for 256^3 and 512^2 for 128^3 . We have verified that this preserves all the information content by comparing the results to the higher resolution projection. Number of stacked projections depends on the box size and ranges between 25 (for τ CDM with $200h^{-1}$ Mpc box) to 150 (for Λ CDM with $50h^{-1}$ Mpc box size).

After the simulation is completed we use the 2-d projections to make maps of SZ. We stack together the maps of SZ separated by the width of simulation box, randomly choosing the center of each box (note that use of periodic

boundary conditions guarantees there is no edge for any of the maps). We then project these maps onto a map constant in angular size. In principle the angular scale of the projection should be determined by the angular scale of the simulation box at the initial z , since any larger scale produces repetition of the same structures in the map. However, most of the structures in the maps are coming from low z and these cover very little volume of the simulation box; hence they do not repeat itself even if we increase the angular scale beyond the size of the box at the highest redshift. Typically we project up to $z \sim 4 - 30$ using oversampling between 1-4 without any noticeable artifacts in the maps. We checked for possible artifacts in the power spectra by comparing weak lensing maps produced in the same way to the analytic predictions [16,17]. The agreement was very good in all models. For SZ it should be even better, since SZ power spectrum is much more dominated by isolated sources and, as will be shown below, large scale correlations do not dominate even on large scales.

A given simulation can be used not only for the simulated parameters, but also for models with lower σ_8 . To do this one can simply relabel an earlier time output as being one at a later time by changing the redshift of projection

$$z^{\text{new}} = (z^{\text{old}} + 1)\sigma_8^{\text{new}}/\sigma_8^{\text{old}} - 1, \quad (2)$$

where superscript old stands for original simulation and new for the new one. Once the redshifts are relabeled one can project over the 2-d projections using the nearest projection to the required z . For a flat model with no cosmological constant this scaling preserves all cosmological parameters (except σ_8). This scaling is particularly useful to obtain the dependence on σ_8 in a flat model independent of other parameters. We verified its accuracy by running two simulations: one with $\sigma_8 = 1$ but using the rescaling of equation 2 to obtain $\sigma_8 = 0.56$ model, and another with $\sigma_8 = 0.56$ at the final output, and found very good agreement between the two. The simulation with $\sigma_8 = 1$ was then used to predict σ_8 dependence of the y parameter and SZ power spectrum.

It is also easy to verify the effect of the baryon density in the limit $\Omega_b \ll \Omega_m$. In this limit the baryons are just a tracer of dark matter potential and do not dynamically couple to it. This fails in the cores of the halos, which are however already not correctly modelled in these adiabatic simulations without cooling and non-thermal energy injection. In this approximation SZ scales linearly with baryon density times Hubble constant $\Omega_b h$. We only show results that are normalized to BBN nucleosynthesis constraint $\Omega_b h^2 = 0.018$, but results for other values of $\Omega_b h$ can be easily obtained using this scaling. Incidentally, one could also use transformation of scale to map a given model into another family of models, this time varying the shape and the amplitude of the input power spectrum. By combining this transformation with the time transformation above one can find a family of models which are normalized to σ_8 today and have a different shape of the power spectrum. The trade-off in this case is a loss in force and mass resolution. Some of the maps produced by the simulations can be found at <http://feynman.princeton.edu/~uros/sz.html>.

III. PRESS-SCHECHTER PREDICTIONS

The Compton parameter $y = \int dy$ is given as a projection over the electron pressure along the line of sight (equation 1). This can be reexpressed as a line of sight integral over the density weighted temperature of electrons,

$$y = \frac{k_B \sigma_T \bar{n}_e}{m_e c^2} \int a^{-2} (1 + \delta_g) T_e d\chi, \quad (3)$$

where δ_g is the gas overdensity and \bar{n}_e mean electron density today.

In Press-Schechter (PS) picture all matter in the universe is divided into halos of a given mass. The mass distribution is specified by the halo density mass function $dn(M)/dM$. This can be written as

$$\frac{dn(M)}{dM} dM = \frac{\bar{\rho}}{M} f(M) dM, \quad (4)$$

where $\bar{\rho}$ is the mean matter density of the universe. The function $f(M)$ denotes the fraction of mass in halos of mass M . It can be expressed in units in which it has a universal form independent of power spectrum or redshift if we express it as a function of peak height $\nu = [\delta_c(z)/\sigma(M)]^2$, where δ_c is the value of a spherical overdensity at which it collapses at z ($\delta_c = 1.68$ for Einstein-de Sitter model) and $\sigma(M)$ is the rms fluctuation in spheres that contain on average mass M at initial time, extrapolated using linear theory to z . For scale free spectra

$$\nu f(\nu) = \frac{M^2}{\bar{\rho}} \frac{dn}{dM} \frac{d \ln M}{d \ln \nu}. \quad (5)$$

The actual form given by Press & Schechter [18] is $\nu f(\nu) = (\nu/2\pi)^{1/2} e^{-\nu/2}$, although modified versions of this form that fit better N-body simulations have been proposed [19]. Direct hydrodynamic simulations have shown good agreement with our form 5 [20].

The virial temperature of the halo in the spherical collapse model is only a function of virial mass and is given by $k_B T_e = qM^{2/3}$. The conversion factor from mass to temperature q is approximately unity if mass is expressed in units of $10^{13}h^{-1}M_\odot$ and T in keV. Density weighted temperature is given by

$$\langle(1+\delta)T\rangle = q \int f(\nu)d\nu M^{2/3}. \quad (6)$$

This gives $\langle(1+\delta)T\rangle = 0.3\text{keV}$ today in a ΛCDM model with $\Omega_m = 0.37$ and $\sigma_8 = 0.8$, with other models giving comparable numbers. Further assuming that gas traces dark matter, ie $\delta_g = \delta$, we can calculate the integrated Compton y parameter from equation 3. This gives $y = 2 \times 10^{-6}$ for this model. Flat models give a factor of 2 lower value because of a more rapid evolution of clusters with z . This reduces y relative to a low density model assuming the cluster abundance today is the same.

Using equation 6 we may also explore the dependence of y on σ_8 . For this we need to relate $\sigma(M)$ to M . Linear power spectrum at the cluster scale can be approximated as a power law $P(k) \propto \sigma_8^2 k^n$. Since rms variance $\sigma^2(M)$ scales as $k^3 P(k)$ one finds $k \propto \nu(\sigma_8^2)^{-2/(n+3)}$. Mass goes as $M \propto \bar{\rho}R^3 \propto k^{-3}$ for which we find $M^{2/3} \propto k^{-2} \propto \sigma_8^{\frac{4}{3+n}}$. On cluster scales we have $-2 < n < -1$, hence $\langle(1+\delta)T\rangle \propto \sigma_8^{2-4}$. The y dependence on σ_8 depends on the projection of $\langle(1+\delta)T\rangle$ along the line of sight (equation 3), but gives qualitatively similar result.

One can also compute power spectrum using the PS model. To do this one can first calculate the 3-d power spectrum of density weighted temperature $P_{(1+\delta)T}(k)$ and then project it along the line of sight using the Limber's equation,

$$C_l = 32\pi^3 \left[\frac{k_B \sigma_T \bar{n}_e}{m_e c^2} \right]^2 \int P_{(1+\delta)T}(k = l/r, a) \frac{d\chi}{a^4 r^2}, \quad (7)$$

where r is the comoving angular distance to χ , given by χ , $R \sinh(\chi/R)$ or $R \sin(\chi/R)$ in a flat, open or closed universe with curvature R , respectively. The above expression is valid in Rayleigh-Jeans limit where $\Delta T/T \equiv j(x)y = -2y$. This can easily be rescaled to another frequency using the spectral function $j(x) = x(e^x + 1)(e^x - 1)^{-1} - 4$ with $x = h\nu/k_B T$ (which in the limit $x \rightarrow 0$ gives $j = -2$).

In the PS formalism there are two contributions to the pressure power spectrum [7–9]

$$P(k) = P^P(k) + P^{hh}(k) \quad (8)$$

The first term $P^P(k)$ arises from the correlations within the single halo. This term contribution to the 3-d power spectrum is given by

$$P_{(1+\delta)T}^P(k) = \frac{q^2}{(2\pi)^3} \int f(\nu)d\nu \frac{M}{\bar{\rho}} M^{4/3} |y(k)|^2, \quad (9)$$

where $y(k)$ is the Fourier transform of the halo profile normalized to unity on large scales ($k \rightarrow 0$), assumed here for simplicity to be independent of M . One power of M above is given by mass pair weighting and $M^{4/3}$ is given by the square of the temperature of the halo. This term is heavily weighted toward rare massive clusters, resulting in a very strong Poisson term compared to the halo-halo correlation term discussed below. As shown in [9] this term dominates over the halo-halo correlation even on large scales, where it behaves as a white noise. In the large scale limit ($k \rightarrow 0$, $y(k) = 1$) the scaling with σ_8 is given by $P_{(1+\delta)T}^P \propto \sigma_8^{14/(3+n)} \propto \sigma_8^{7-14}$. This will again be modified somewhat by the integration over the redshift, but does provide qualitative understanding for the strong σ_8 dependence seen in the simulations described below.

Second term is the contribution from halos correlated with one another. On large scales these cluster according to the linear power spectrum $P_{\text{lin}}(k)$, except that they can be biased relative to the dark matter. The halo bias can be either larger than unity for halos more massive than the nonlinear mass or less than unity for those below that. An expression that fits N-body simulations reasonably well was given in [8,21] (see also [19,22] for a modification relevant for lower mass halos)

$$b(\nu) = 1 + \frac{\nu - 1}{\delta_c}. \quad (10)$$

The halo-halo contribution to the density weighted T power spectrum is given by

$$\begin{aligned} P_{(1+\delta)T}^{hh}(k) &= P_{\text{lin}}(k) \left[q \int f(\nu)d\nu M^{2/3}(\nu) b(\nu) y(k) \right]^2 \\ &\equiv P_{\text{lin}}(k) [\langle b \rangle_{(1+\delta)T} \langle (1+\delta)T \rangle]^2, \end{aligned} \quad (11)$$

where $\langle b \rangle_{(1+\delta)T}$ is the pressure weighted bias, defined as

$$\langle b \rangle_{(1+\delta)T} \equiv \frac{\int f(\nu) d\nu M^{2/3}(\nu) b(\nu) y(k)}{\int f(\nu) d\nu M^{2/3}(\nu) y(k)}. \quad (12)$$

For Λ CDM model we find in the large scale limit ($y = 1$) $\langle b \rangle_{(1+\delta)T} = 3$, hence SZ halos are significantly biased relative to the dark matter. This is because the $T \propto M^{2/3}$ weighting weights preferentially towards the large halo masses which are biased. The bias decreases towards smaller scales where $y(k)$ suppression for finite k is more important for larger more massive halos and the dominant contribution shifts towards smaller, unbiased or antibiased halos. Despite this large bias the halo correlation term is small relative to the halo term even on large scales and Press-Schechter model predicts that SZ power spectrum does not trace large scale structure on large scales.

If SZ does not trace LSS, the large scale bias b cannot be measured from its power spectrum. Cross-correlating SZ with weak lensing or galaxy map is a more promising way to obtain this large scale bias. This is because the Poisson term is given by $M^{5/3}$ weighting,

$$P_{(1+\delta)T,\delta}^P(k) = \frac{q}{(2\pi)^3} \int f(\nu) d\nu \frac{M}{\bar{\rho}} M^{2/3} |y(k)|^2, \quad (13)$$

and is so less dominated by rare objects than SZ power spectrum with $M^{7/3}$ weighting. The correlated contribution to the cross-correlation between density weighted T and dark matter density is given by

$$\begin{aligned} P_{(1+\delta)T,\delta}^{hh}(k) &= P_{\text{lin}}(k) \left[q \int f(\nu) d\nu M^{2/3} b(M) \right] \left[\int f(\nu) d\nu b(M) \right] \\ &= P_{\text{lin}}(k) \langle b \rangle_{(1+\delta)T} \langle (1+\delta)T \rangle, \end{aligned} \quad (14)$$

where the second integral above is the mass weighted bias, which is by definition unity. Numerical comparison between the two terms indeed shows that they are comparable on large scales. To obtain the SZ-weak lensing or galaxy cross-correlation power spectrum we again use this 3-d power spectrum in Limber's equation 7 with the appropriate window function for the dark matter or galaxy projection.

IV. SIMULATION RESULTS

A. Mean Compton parameter

We first present the results on the mean y parameter. The value for this parameter is 1.0×10^{-6} for τ CDM in $100h^{-1}$ Mpc simulations with 128^3 mesh, 2.4×10^{-6} for O CDM in $100h^{-1}$ Mpc with 256^3 mesh and 2.0×10^{-6} for Λ CDM with $100h^{-1}$ Mpc with 256^3 mesh or $50h^{-1}$ Mpc with 128^3 mesh. For the latter y decreases by roughly 20% if the resolution is decreased to 128^3 mesh, suggesting that small halos not resolved in larger box simulations contribute a significant fraction to its value. This is also confirmed by Press-Schechter type calculations [7]. Non-thermal energy injection and cooling may provide additional corrections to the results of the adiabatic simulations. For example, [23] include feedback in their simulations and find significantly higher density averaged temperature (1keV) than our simulations (0.3keV), although other simulations that also include heating do not (G. Bryan, private communication). The mean y parameter is therefore sensitive to the thermal history of the gas.

Our results are still one order of magnitude below the current experimental limits from COBE/FIRAS $y < 1.5 \times 10^{-5}$ [6], so it is unlikely that this constraint will play a major role in distinguishing between the models that differ in the history of energy injection in the universe. On the other hand mean y parameter does put a constraint on the σ_8 . This scaling of y with σ_8 can be obtained from the same simulation using the method described in previous section. We find $y \propto \sigma_8^{3-4}$, which is in a good agreement with the Press-Schechter predictions. To violate the FIRAS limits one needs to increase σ_8 by a factor of 2 over the cluster abundance value. COBE normalized standard CDM with $\sigma_8 = 1.3$ would be problematic. Our results are a factor of 2 lower from those in [13] for the two low density models (once we account for the difference in $\Omega_b h$), while we are in a good agreement for τ CDM model. This disagreement does not seem to be explained by limited mass resolution on small scales, since our simulations have higher mass and force resolution, yet predict lower values for y for the low density models. We agree well with results in [15].

B. SZ power spectrum

Next we explore the power spectra of SZ in the Rayleigh-Jeans regime. We first investigate the effects of resolution. These are shown in figure 1 for different parameters of the simulation for Λ CDM model. Shown are 256^3 $100h^{-1}$ Mpc simulation, 128^3 $100h^{-1}$ Mpc simulation, 128^3 $200h^{-1}$ Mpc simulation and 128^3 $50h^{-1}$ Mpc simulation. They all agree on large scales, where the shape is close to the white noise model, characteristic of a power spectrum dominated by rare sources. On small scales $200h^{-1}$ simulation begins to loose power for $l > 1000$ compared to other simulations. Comparison between 128^3 and 256^3 $100h^{-1}$ Mpc shows that the two are in good agreement on scales up to $l \sim 1500$, beyond which 128^3 begins to loose power. Similar conclusion is obtained by comparing $50h^{-1}$ Mpc and $100h^{-1}$ Mpc both with 128^3 . The figure shows that a $50h^{-1}$ Mpc box is sufficient for the power spectrum on large scales. This indicates that the large scale power spectrum is not dominated by very massive clusters above $10^{15}M_{\odot}$ which do not form in such small boxes, but rather by less massive $10^{14-15}M_{\odot}$ clusters, which happen to be nearby in the projection along the line of sight. This conclusion is also confirmed by the Press-Schechter calculation, where the brightest sources correspond to this mass range. On small scales the $50h^{-1}$ Mpc box has a power spectrum comparable to 256^3 $100h^{-1}$ Mpc simulation with the same mass and force resolution. Very little small scale power therefore arises from mode-mode coupling with scales larger than $50h^{-1}$ Mpc. Overall $100h^{-1}$ Mpc 256^3 simulation resolves the power spectrum between $100 < l < 5000$, while 128^3 simulations of the same size are sufficient between $100 < l < 2000$.

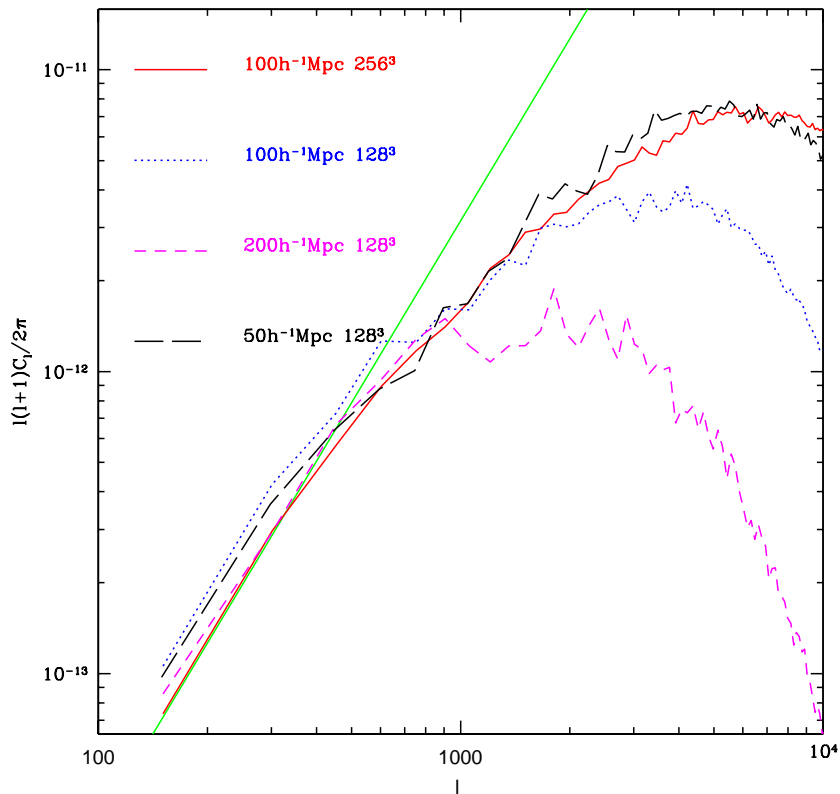


FIG. 1. Power spectrum comparison between different resolution and box size simulations for Λ CDM model. Also shown is the white noise spectrum scaling as l^2 . On large scales the SZ spectrum is white noise in all cases.

On large scales the power spectrum approaches white noise in slope. This is an indication that the power spectrum is dominated by the rare bright sources in the map and not by the correlations between them, which would give a much shallower slope. The same behaviour is seen also in other cosmological models, shown in figure 2. While $OCDM$ gives similar predictions to Λ CDM model, τ CDM is significantly lower, just like in the case of mean y parameter. Low density Λ CDM predicts 3×10^{-7} fluctuations around $l \sim 100$, which rises to 3×10^{-6} at $l \sim 5000$. Comparison with primary CMB in figure 2 shows that the SZ is unlikely to contaminate CMB power spectrum for MAP, while Planck and smaller scale experiments should be able to measure the SZ power spectrum. Our results are in good agreement with [15], although we note that our $OCDM$ spectrum is somewhat higher than theirs, in better agreement with the

PS calculations.

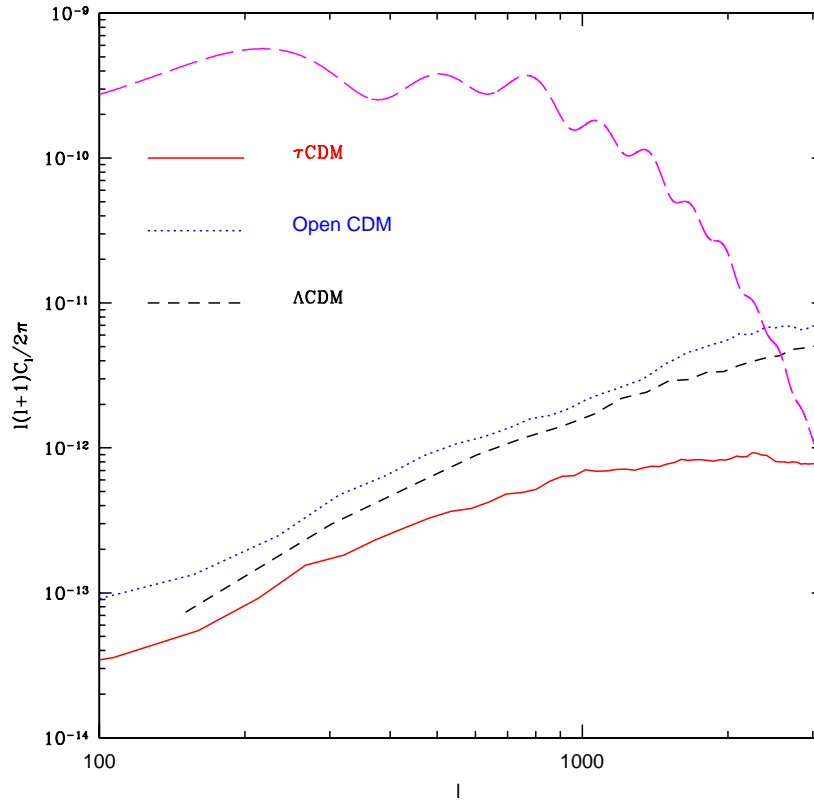


FIG. 2. Power spectrum comparison between cluster normalized τCDM , λCDM and $OCDM$. The latter two have significantly more power. Also shown is the primary CMB (long dashed) which dominates on large scales.

Figure 3 shows field to field variations in the power spectrum for $2^\circ \times 2^\circ$ maps. It shows significant fluctuations on large scales. This is another indication that the power spectrum on large scales is dominated by rare bright sources. On smaller scales the power spectrum is more robust. The main contribution on those scales is from smaller more abundant halos, so there is less sampling variance. Note that as the map size increases the chance of finding a bright source in it increases as well, so the median power spectrum on large scales grows with the map size. This is equivalent to the power spectrum after the brightest sources have been removed. The power spectrum in a typical few degree map should correspond to the power spectrum with a few thousand brightest sources removed. As shown in [9] this can reduce the power spectrum on large scales significantly and should be kept in mind when comparing our results to other predictions. For example, power spectra in [15] are based on all the power without the removal of bright sources, which should in general give a higher amplitude on large scales.

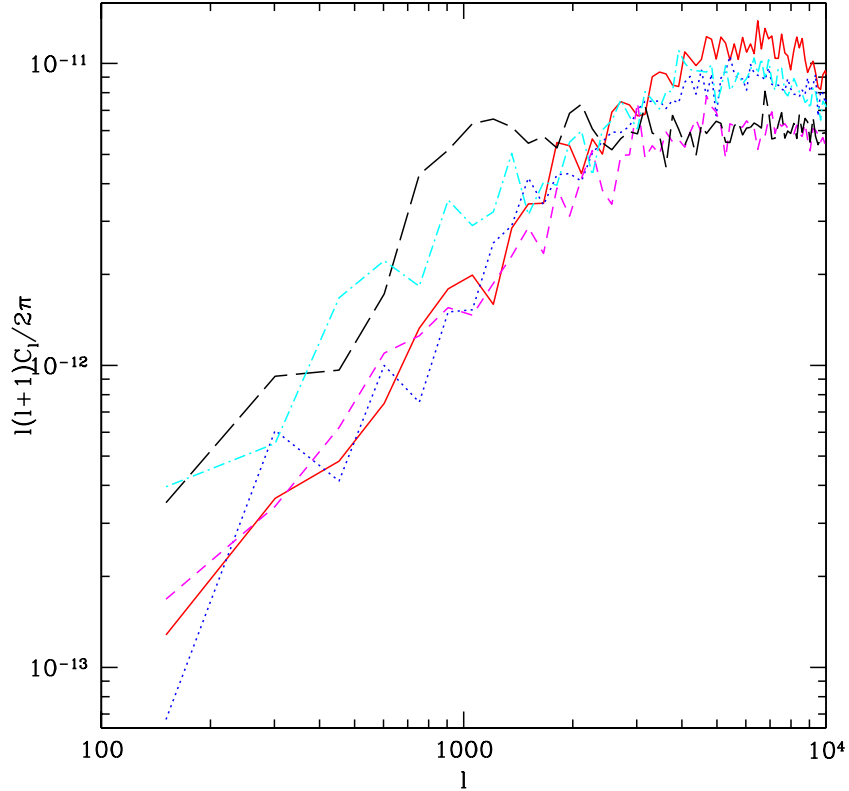


FIG. 3. Power spectrum variations for several $2^\circ \times 2^\circ$ fields in λ CDM model. There are a factor of 2 variations from field to field even on large scales, caused by rare bright objects in the map.

Figure 4 shows the change in the power spectrum as a function of σ_8 for τ CDM model. The amplitude of the power spectrum is very sensitive to σ_8 . Doubling this parameter changes the power spectrum by 2 orders of magnitude. Fitting to a power law we find $C_l \propto \sigma_8^7$. This steep dependence on σ_8 can be understood with Press-Schechter formalism developed in §3 and is caused by a rapid increase in number of bright sources as a function of σ_8 , and is in contradiction to the estimates of [12]. One can also see a crude estimate of the scaling relation by noting that the $C_l \propto \langle T \rangle \delta^2$ and the temperature is a function of the non-linear length scale r_{NL} , i.e. $T \propto (r_{\text{NL}} H_0)^2$ [23]. For CDM like spectra near the non-linear mass scale we have $r_{\text{NL}} \propto \sigma_8^{1-2}$, giving $C_l \propto \sigma_8^{6-8}$, similar to what we find in simulations and to the PS arguments. This indicates that care must be exercised when extracting cosmological parameters from SZ maps, since similar differences arise between low and high density cosmological models (figure 2). A small increase in σ_8 of the order of 20% changes the spectrum as much as does changing the density from $\Omega_m = 1$ to $\Omega_m = 0.3$. Unless we are confident that we know the local value of σ_8 to better than this accuracy we cannot use SZ to infer the density of the universe. Similar argument also explains the redshift dependence of SZ power spectrum, which is very strong. Most of the contribution to the power spectrum comes from $z < 1$. This is also true in Λ CDM, although the z dependence is less steep there.

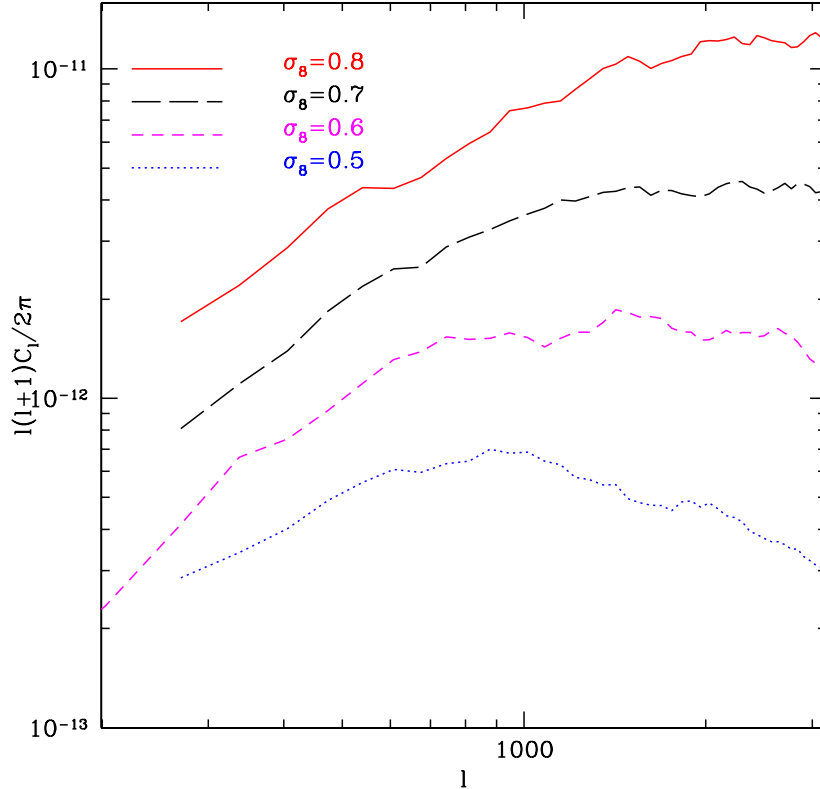


FIG. 4. Dependence of SZ power spectrum on σ_8 in τ CDM model.

C. Non-Gaussian signatures

Since we have 2-d maps of SZ we may use these to study non-Gaussian signatures in SZ. There are two reasons why to investigate non-Gaussian signatures of SZ. First is that such information can be used to determine the cosmological model. Example of this is the SZ luminosity function, where one identifies SZ sources and plots the number density as a function of the flux in SZ [13]. The abundance of such sources in the limit where they are unresolved has been made by the Press-Schechter formalism [5,24] or peak-patch formalism [25]. It has been shown that the number density of sources is strongly sensitive to the density parameter, similar to the mean y and power spectrum statistics discussed above. However, the sources have some internal structure, they may be clustered, may contain substructure and may not be spherical, all of which complicates such analytic approaches and they need to be verified using the simulations. This is of particular interest to the proposed surveys of small fields centered on a random portion of the sky [4] which will not in general detect massive clusters, but rather a collection of smaller sources. Simulations such as these presented here are necessary for investigation of the non-Gaussian effects in such random portions of the sky.

Second reason to study non-Gaussian signatures is that they may provide additional leverage in separating the SZ from the primary CMB, at least under the assumption that primary CMB is Gaussian. Even when one does not have sufficient frequency coverage to distinguish the two components on the basis of their different frequency dependence one can use non-Gaussian signature of SZ to estimate its contribution to the power spectrum. The only assumption in this procedure is that at a given smoothing scale there is a strong correlation between the non-Gaussian signature and its second moment, so that the latter can be estimated from the former.

It was shown above that the 2-point statistics is dominated by rare bright sources and so is very noisy on large scales. This will be even worse if one considers higher order statistics such as skewness and kurtosis. For this reason we concentrate here on the one point distribution function (pdf) of SZ smoothed at a given angular scale. These are shown in figure 5 for a $2^\circ \times 2^\circ$ field in Λ CDM model with several smoothing radii, all smoothed with a top-hat window. As shown in figure 5 the pdf is approximately lognormal on small scales, in the sense that there is an excess of large y decrements caused by bright rare sources. The pdf can be transformed into an approximate Gaussian if plotted against $\log(y)$. For larger smoothing angles the pdf becomes narrower and approaches a Gaussian, so it

becomes more difficult to distinguish it from primary CMB on this basis.

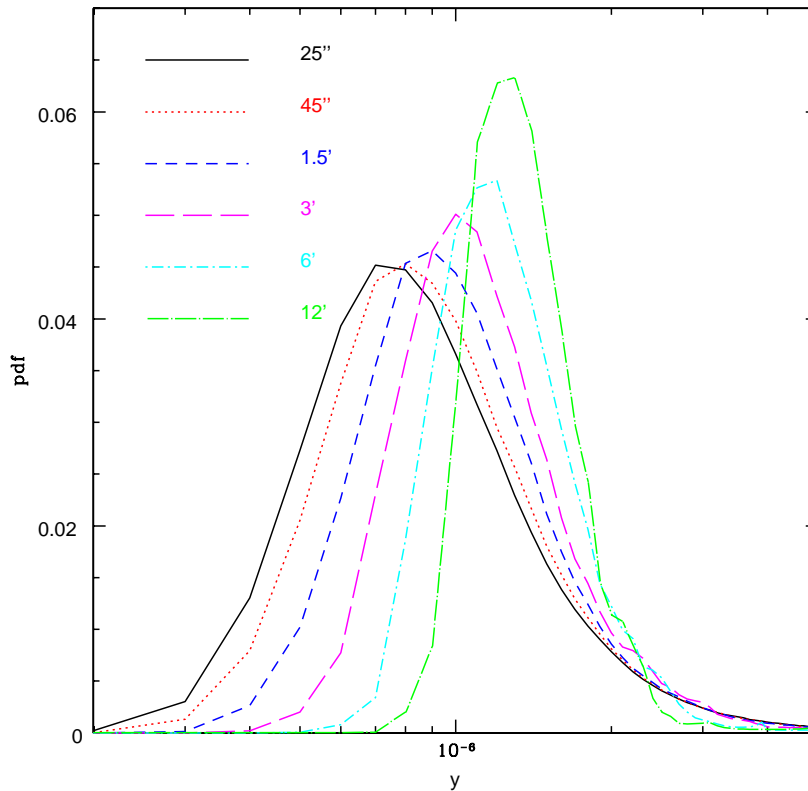


FIG. 5. The one point distribution function of $\log y$ for several smoothing radii with a top-hat window.

D. SZ-weak lensing and galaxy cross-correlation

SZ map can be cross-correlated with other maps, such as weak lensing, galaxy or X-ray maps. The first two are sensitive to projected density and may not be so strongly dominated by rare bright objects, while the latter traces projected $\rho^2 T^{1/2}$ and is even more strongly dominated by rare objects than SZ. Examples of weak lensing maps are those reconstructed from shape distortions of $z \sim 1$ galaxies or from CMB distortions at $z \sim 1100$. Example of projected galaxy maps are those from APM, SDSS or from numerous degree field surveys. They can be parametrized by the mean galaxy redshift. In the case of SDSS one can use photometric information to weight the galaxies according to their distance to optimize the signal to noise of the cross-correlation. Even more promising are smaller and deeper surveys, such as those used for weak lensing studies with several hundred thousand galaxies over a degree area.

A useful quantity to compare the cross-correlation between different maps is to compute the cross-correlation coefficient

$$\text{Corr}(l) = \frac{C_{SZ,X}(l)}{[C_{SZ}(l)C_X(l)]^{1/2}}. \quad (15)$$

Figure 6 shows the cross-correlation coefficient for weak lensing map reconstructed from background galaxies at $z = 0.5, 1, 1100$. The cross-correlation coefficients for all 3 cases is between 0.4 and 0.6 and only weakly depends on scale. Similar results are also obtained if one cross-correlates SZ with a galaxy catalog with a mean redshift of $z \sim 0.2 - 0.5$. This result shows that both SZ and weak lensing maps are dominated by relatively nearby objects, which is why the cross-correlation coefficient does not significantly decrease as the redshift of background galaxies is decreased. This is good news for shallow surveys such as SDSS, which should be able to detect the cross-correlation signal when compared to MAP or Planck maps.

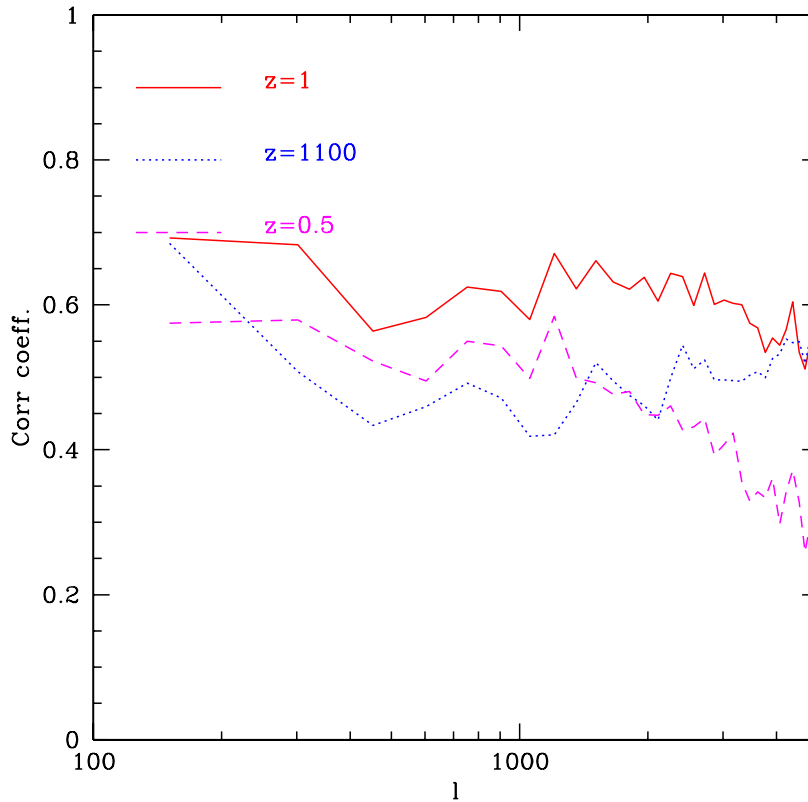


FIG. 6. Cross-correlation coefficient between SZ and weak lensing convergence assuming background source is at $z = 0.5, 1, 1100$. Similar results are obtained for cross-correlation with galaxies whose mean distance is at half the distance to the lens source.

The amplitude of the cross-correlations can also be compared to the analytic predictions developed in §3 and we find good agreement between the two. The predictions have also been made in the case of weak lensing of CMB by [26,27]. Our results are several times lower on scales between $100 < l < 3000$. A more detailed comparison shows that the assumed bias in the two models is comparable ($b \sim 3 - 4$) and the difference is mostly caused by lower density weighted temperature in our simulations (0.3keV), consistent with PS, compared to their assumption (1keV). Density weighted temperature is sensitive to the thermal injection from stars and supernovae and it could be significantly higher than in our simulations, which neglect this effect. However, such heating of the gas would shift the weight in SZ to cooler halos (below 1keV), which are not biased or are even antibiased. So non-thermal increase in density weighted temperature also requires a decrease in bias and the two effects nearly cancel out, leading to a smaller sensitivity of the cross-correlation power spectrum on the density weighted temperature than one would naively assume. Unfortunately this also implies that the expected signal to noise of SZ and CMB cross-correlation will be significantly lower than predicted [26,27] and becomes only marginal using our results.

V. DISCUSSION AND CONCLUSIONS

Using hydrodynamical simulations we have produced maps of SZ and analyzed some of their low order statistics. The mean Compton parameter was found to be in the range $\bar{y} \sim 1 - 2.5 \times 10^{-6}$, an order of magnitude below current FIRAS limits. Only if one increases σ_8 by a factor of 2 over the cluster abundance constraint does one violate the FIRAS limit, something which is clearly excluded based on cluster abundance data. FIRAS limits will therefore not play a major role in constraining the cosmological models.

The power spectra were found to be noisy and white noise like on large scales, indicating that they are dominated

by uncorrelated bright sources. The amplitude at $l \sim 1000$ is $1 - 3 \times 10^{-6}$ and does not represent a major source of foreground to primary CMB on large scales ($l < 1000$). On smaller scales SZ power spectrum should be detectable and should dominate over CMB for $l > 2000$. On these scales the predictions become sensitive to the thermal energy injection into the gas and simulations that ignore such effects become unreliable. Conversely, power spectrum of SZ on small scales should give us important information on the thermal history of the gas in small halos. Note that the dominant contribution to the power spectrum comes from relatively nearby structures with $z < 1$, so SZ will not provide information on gas history at high z .

On scales where SZ is not negligible compared to primary CMB one can use the non-Gaussian signatures of SZ to estimate its contribution to the power spectrum. We have shown that on arcminute scales the one point distribution function is well approximated as a log-normal, differing significantly from a normal distribution. This signature can be used to estimate the contribution of SZ to the power spectrum even in the absence of multifrequency information.

Further insight into the thermal history of the gas can be obtained by cross-correlating SZ with other maps that trace large scale structure, such as weak lensing or projected galaxy map. This can also provide information on correlations between groups and clusters on large scales and their bias relative to dark matter. The cross-correlation coefficient is quite high, of order 0.5, across a wide range of scales even when the redshift distribution of galaxies or lensing mass peaks well below $z \sim 1$. This strong correlation provides further incentive to planned SZ surveys on random patches of the sky, since even if sensitivity is not sufficient to detect SZ directly, one may be able to detect it through cross-correlation with weak lensing or galaxy maps, thus providing information on the thermal state of the gas in the universe.

We thank Eiichiro Komatsu, Alexandre Refregier and David Spergel for useful correspondence. U.S. acknowledges the support of NASA grant NAG5-8084. Computing support from the National Center for Supercomputing Applications is acknowledged.

- [1] R. A. Sunyaev and Ya. B. Zel'dovich, Ya.B., *Comm. Astrophys. Space Phys.* **4**, 173 (1972); R. A. Sunyaev and Ya. B. Zel'dovich, *Ann. Rev. Astron. Astrophys.* **18**, 357 (1980).
- [2] Y. Rephaeli, *Ann. Rev. Astron. Astrophys.* **33**, 541 (1995).
- [3] M. Birkinshaw, *Phys. Rept.* **310**, 97 (1999).
- [4] J. E. Carlstrom, M. K. Joy, L. Grego, G. P. Holder, W. L. Holzapfel, J. J. Mohr, S. Patel and E. D. Reese, in *Nobel Symposium Particle Physics and the Universe*, to appear in *Physica Scripta* and *World Scientific*, eds. L. Bergstrom, P. Carlson and C. Fransson, preprint astro-ph/9905255.
- [5] Aghanim, A. De Luca, F. R. Bouchet, R. Gispert and J. L. Puget, *Astron. Astrophys.* **325**, 9 (1997).
- [6] D. J. Fixsen, E. S. Cheng, J. M. Gales, J. C. Mather, R. A. Shafer and E. L. Wright, *Astrophys. J.* **473**, 576 (1996).
- [7] F. Atrio-Barandela and J. P. Mücke, *Astrophys. J.* **515**, 465 (1999).
- [8] S. Cole and N. Kaiser, *Mon. Not. Roy. Astron. Soc.* **233** 637 (1988).
- [9] E. Komatsu and T. Kitayama, *Astrophys. J. Lett.* **526**, L1 (1999).
- [10] U. Pen, *Astrophys. J. Suppl.* **115**, 19 (1998).
- [11] P. A. Thomas, and R. G. Carlberg, *Mon. Not. Roy. Astron. Soc.* **240**, 1009 (1989).
- [12] R. Scaramella, R. Cen and J. P. Ostriker, *Astrophys. J.* **416**, 399 (1993).
- [13] A. da Silva, D. Barbosa, D., A. R. Liddle and P. A. Thomas, *Mon. Not. R. Astron. Soc.* (submitted), astro-ph/9907224.
- [14] F. M. Persi, D. N. Spergel, R. Cen and J. P. Ostriker, *Astrophys. J.* **442**, 1 (1995).
- [15] Refregier, A., Komatsu, E., Spergel, D. N., & Pen, U., *Phys. Rev. D.* (submitted).
- [16] B. Jain, and U. Seljak, *Astrophys. J.* **484**, 560 (1997).
- [17] B. Jain, U. Seljak and S. White, *Astrophys. J.* , ??? (1999).
- [18] W. H. Press and P. Schechter, *Astrophys. J.* **187**, 425 (1994).
- [19] R. K. Sheth and G. Tormen, *Mon. Not. Roy. Astron. Soc.* **308**, 119 (1999).
- [20] U. Pen, *Astrophys. J.* **498**, 60 (1998).
- [21] H. J. Mo and S. D. M. White, *Mon. Not. Roy. Astron. Soc.* **282**, 347 (1996).
- [22] Y. P. Jing, *Astrophys. J.* **515**, 45 (1999).
- [23] R. Cen and J. Ostriker, *Astrophys. J.* **514**, 1 (1999).
- [24] D. Barbosa, J. G. Bartlett, A. Blanchard and J. Oukbir, *Astron. Astrophys.* **314**, 13 (1996).
- [25] J. R. Bond and S. T. Myers, *Astrophys. J. Suppl.* **103**, 63 (1996).
- [26] D. M. Goldberg and D. N. Spergel, *Phys. Rev. D* **59** 3002 (1999).
- [27] A. R. Cooray and W. Hu, *Astrophys. J.* (submitted), astro-ph/9910397

This figure "szlam.gif" is available in "gif" format from:

<http://arxiv.org/ps/astro-ph/0001120v1>

This figure "szopen.gif" is available in "gif" format from:

<http://arxiv.org/ps/astro-ph/0001120v1>

This figure "sztau.gif" is available in "gif" format from:

<http://arxiv.org/ps/astro-ph/0001120v1>